Human Molecular Genetics, 2013, Vol. 22, No. 11 **2186–2199**
doi:10.1093/hmg/ddt071
Advance Access published on February 12, 2013

Epileptogenic Q555X SYN1 mutant triggers imbalances in release dynamics and short-term plasticity

Gabriele Lignani[1,2], Andrea Raimondi[1], Enrico Ferrea[1], Anna Rocchi[1], Francesco Paonessa[1], Fabrizia Cesca[1], Marta Orlando[1,2], Tatiana Tkatch[1], Flavia Valtorta[3], Patrick Cossette[4], Pietro Baldelli[1,2] and Fabio Benfenati[1,2,*]

[1]Department of Neuroscience and Brain Technologies, Istituto Italiano di Tecnologia, Via Morego 30, Genova 16163, Italy, [2]Department of Experimental Medicine, University of Genova, Viale Benedetto XV, 3, Genova 16132, Italy [3]San Raffaele Scientific Institute and Vita-Salute University, Via Olgettina 58, Milano 20132, Italy and [4]Centre for the Study of Brain Diseases, University of Montreal, Quebec, Canada

Received January 9, 2013; Revised and Accepted February 8, 2013

Synapsin I (SynI) is a synaptic vesicle (SV) phosphoprotein playing multiple roles in synaptic transmission and plasticity by differentially affecting crucial steps of SV trafficking in excitatory and inhibitory synapses. SynI knockout (KO) mice are epileptic, and nonsense and missense mutations in the human SYN1 gene have a causal role in idiopathic epilepsy and autism. To get insights into the mechanisms of epileptogenesis linked to SYN1 mutations, we analyzed the effects of the recently identified Q555X mutation on neurotransmitter release dynamics and short-term plasticity (STP) in excitatory and inhibitory synapses. We used patch-clamp electrophysiology coupled to electron microscopy and multi-electrode arrays to dissect synaptic transmission of primary SynI KO hippocampal neurons in which the human wild-type and mutant SynI were expressed by lentiviral transduction. A parallel decrease in the SV readily releasable pool in inhibitory synapses and in the release probability in excitatory synapses caused a marked reduction in the evoked synchronous release. This effect was accompanied by an increase in asynchronous release that was much more intense in excitatory synapses and associated with an increased total charge transfer. Q555X-hSynI induced larger facilitation and post-tetanic potentiation in excitatory synapses and stronger depression after long trains in inhibitory synapses. These changes were associated with higher network excitability and firing/bursting activity. Our data indicate that imbalances in STP and release dynamics of inhibitory and excitatory synapses trigger network hyperexcitability potentially leading to epilepsy/autism manifestations.

INTRODUCTION

Synapsins (Syns) are synaptic vesicle (SV) phosphoproteins that play multiple roles in synaptic transmission and plasticity (1). Syns are implicated in the regulation of SV trafficking between the reserve pool (RP) and the readily releasable pool (RRP) and in facilitating the post-docking steps of release. Although widely expressed, Syns differentially affect crucial steps of presynaptic physiology in excitatory and inhibitory synapses. An impairment of inhibitory function and a facilitated excitatory transmission were observed in mice constitutively lacking SynI, SynII, SynI/II or SynI/II/III, resulting in network hyperexcitability (2–6). This aspect is particularly interesting because dysfunctions of GABAergic neurons and an excitation/inhibition (E/I) imbalance contribute to numerous neuropsychiatric phenotypes, including epilepsy, autism spectrum disorder (ASD) and Rett's syndrome (7–11). Accordingly, the same strains of Syn knockout (KO) mice display an overt epileptic phenotype associated with behavioral disturbances, including specific defects in social interactions suggestive of an ASD phenotype (12,13).

*To whom correspondence should be addressed. Tel: +39 01071781434; Fax: +39 01071781230; Email: fabio.benfenati@iit.it

Nonsense and missense mutations in SYN1 were recently identified in epileptic and ASD patients (14), strengthening the hypothesis that a disturbance of synaptic homeostasis underlies the pathogenesis of both diseases. Because SynI is a key regulator of SV trafficking and short-term plasticity (STP) with distinct roles in inhibitory and excitatory synapses (2–5), an alteration of its function could differentially affect the STP responses of excitatory and inhibitory synaptic transmission.

We used patch-clamp electrophysiology coupled to electron microscopy and multi-electrode arrays (MEA) to define the physiological impact of the Q555X mutation at excitatory and inhibitory terminals of primary SynI KO hippocampal neurons in which either wild-type (WT) or mutant human SynI (hSynI) was expressed by lentiviral transduction. We identified distinct physiological changes in quantal parameters, release dynamics and STP at inhibitory and excitatory synapses. A decrease in synchronous glutamate and GABA release was paralleled by an increase in asynchronous release that was much more intense in excitatory synapses and by an excitation/inhibition (E/I) imbalance in response to STP paradigms. These imbalances triggered an overt hyperexcitability compatible with a causal role of Syn I mutations in the development of epilepsy and ASD.

RESULTS

Q555X-hSynI differentially affects SV distribution in inhibitory and excitatory terminals

To test the physiological effects of the mutation, we investigated whether the expression of Q555X-hSynI could alter the density and ultrastructure of excitatory and inhibitory synapses. Mouse and human SynI are highly homologous, and reintroduction of hSynI was found to rescue the defects in SV trafficking of SynI KO neurons (14). Primary SynI KO hippocampal neurons were infected with lentiviral vectors encoding for either WT- or Q555X-hSynI. Analysis of green fluorescent protein (GFP) immunostaining showed that the vast majority of the neurons (80–90%) were transduced and that the overall expression levels of WT- and Q555X-hSynI isoforms were comparable (Fig. 1A; Supplementary Material, Fig. S1). As previously reported (14), the nerve terminal targeting of hSynI was not affected by the Q555X mutation. Colocalization analysis of hSynI with the presynaptic marker's vesicular GABA transporter (VGAT) and vesicular glutamate transporter-1 (VGLUT1) also revealed no differences in the GFP intensity in both inhibitory and excitatory terminals expressing either WT- or Q555X-hSynI (Fig. 1A and B). Moreover, the expression of either hSynI isoform had no effect on the density of excitatory and inhibitory synapses labeled by VGLUT1 and VGAT, respectively (Fig. 1A and C) or on the ratio between excitatory and inhibitory synapses (Supplementary Material, Fig. S1).

Electron microscopy was used to evaluate the density and distribution of SVs in presynaptic terminals from 'asymmetric' excitatory and 'symmetric' inhibitory synapses expressing either WT- or Q555X-hSynI (Fig. 1D–I). Both excitatory and inhibitory terminals expressing Q555X-hSynI exhibited a general architecture similar to WT-hSynI-positive synapses (Fig. 1D and E). Morphometric analysis showed a significantly decreased total SV density in inhibitory terminals expressing Q555X-hSynI with respect to WT-hSynI terminals, an effect that was mostly due to a marked reduction in the pool of SVs more distant from the active zone (AZ; Fig. 1F). On the contrary, expression of Q555X-hSynI did not affect either the total SV density or the SV distribution in excitatory synapses (Fig. 1G). Although the number of docked SVs in inhibitory synapses expressing Q555X-hSynI was not affected (Fig. 1H), the expression of Q555X-hSynI increased the number of docked SVs in excitatory synapses (Fig. 1I).

Q555X-hSynI equally impairs excitatory and inhibitory basal transmission

Next, we investigated whether the expression of Q555X-hSynI could alter the functional properties of excitatory and inhibitory synapses. Because SynI plays pre- and post-docking roles in synaptic transmission (2–4,15,16), we analyzed single-evoked inhibitory (eIPSCs) and excitatory post-synaptic currents (eEPSCs) in WT-hSynI and Q555X-hSynI expressing neurons. In both synapse types, Q555X-hSynI expression was associated with a decrease in the amplitude of single eIPSCs and eEPSCs and a parallel increase in latency, suggesting a potential alteration of the SV fusion mechanisms (Fig. 2A and B; Table 1).

No changes in miniature EPSC (mEPSC) and miniature IPSC (mIPSC) amplitude, as well as in their rise and decay times, were observed in synapses expressing either WT-hSynI or Q555X-hSynI (Fig. 2C and D; Table 1), thus excluding post-synaptic effects. However, whereas mIPSCs frequency was not affected, mEPSC frequency was significantly decreased in Q555X-hSynI synapses (Fig. 2D). Quantal size and PSC kinetics were unaffected in all cases, whereas the coefficient of variation (CV) of eEPSC amplitudes was selectively increased. Because the number of excitatory synapses was unchanged, these results suggest that a reduction in the probability of release (Pr) may occur at Q555X-hSynI excitatory synapses.

Q555X-hSynI differentially affects release dynamics at inhibitory and excitatory synapses

Synchronous neurotransmitter release is directly coupled with action potentials (APs), whereas asynchronous release is a delayed release due to Ca^{2+} accumulation in the presynaptic terminal, following a train of APs (17–19). Cumulative amplitude and cumulative charge analyses were performed to calculate Pr and the size of synchronous RRP (RRP_{syn}) and asynchronous release, respectively (Fig. 3A–D; Supplementary Material, Fig S2).

Although Pr was not affected in inhibitory synapses expressing Q555X-hSynI, it was significantly decreased in excitatory synapses (Fig. 3E and F), as expected from the CV analysis (Table 1). In inhibitory synapses, Q555X-hSynI markedly decreased RRP_{syn} and concomitantly increased the asynchronous charge (Fig. 3E). Due to these opposite effects, no differences were observed in the total charge RRP (RRP_{tot}; Fig. 3C and E). In excitatory synapses, Q555X-hSynI did not change the size of RRP_{syn}, but strongly increased the asynchronous

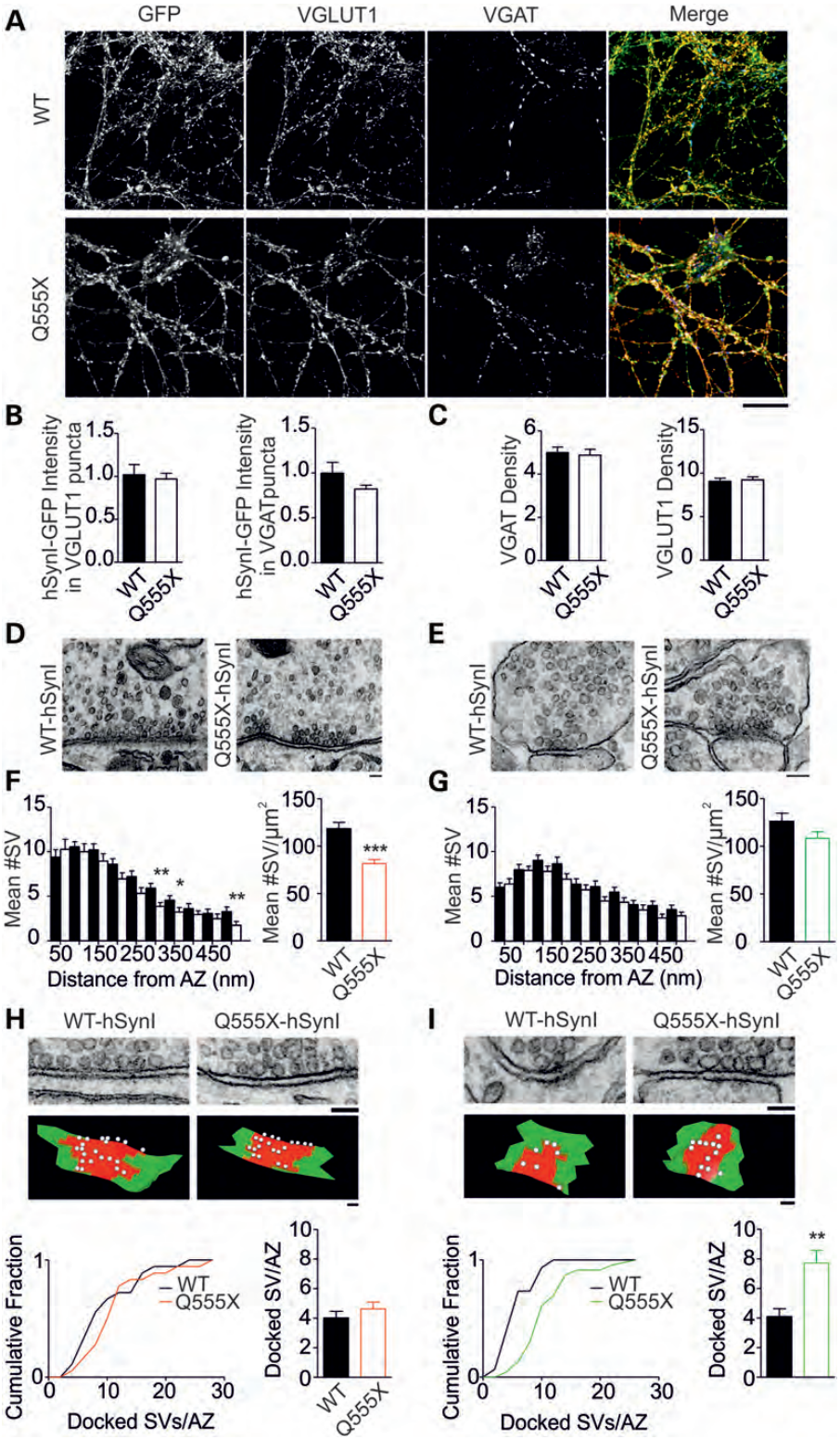

Figure 1. Expression of mutant hSynI alters SV distribution in presynaptic terminals. (**A**) Expression and distribution of the GFP-labeled hSynI in inhibitory and excitatory terminals labeled with anti-VGAT and anti-VGLUT1 antibodies. Scale bar, 20 μm (**B**) Quantitative evaluation of GFP fluorescence performed in triple-stained cultures transduced with either WT- or Q555X-hSynI. The intensity of the GFP signal colocalizing with VGAT- and VGLUT1-positive puncta is expressed in percentage of the WT-SynI values as means ± SEM ($n = 30$ and $n = 25$ for WT- and Q555X-hSynI, respectively). (**C**) Effects of the expression of either WT- or Q555X-hSynI on the mean (± SEM) density of VGAT- and VGLUT1-positive puncta ($n = 30$ and $n = 25$ for WT- and Q555X-hSynI, respectively). (**D**–**G**) Morphometric analysis of SV distribution performed on electron micrographs obtained from inhibitory (D) and excitatory (E) synapses transduced with either WT- or Q555X-hSynI. Scale bar, 100 nm. The overall SV density and the frequency distribution of SVs in shells at increasing distance from the

charge during the train (Fig. 3F), resulting in a 2-fold increase in RRP_{tot} in Q555X-hSynI synapses (Fig. 3D and F). The net increase in the total RRP in excitatory synapses, together with the substantial preservation of total RRP of inhibitory synapses (Fig. 3E and F), demonstrates a good correlation between the RRP size calculated using the cumulative total charge analysis and the number of docked SVs evaluated by electron microscopy (see Fig. 1H and I). Taken together, the results show that the Q555X mutation decreases synchronous release in both inhibitory and excitatory synapses, albeit with distinct mechanisms, and increases asynchronous release in both synapse types, but with a much stronger effect on excitatory synapses, leading to an overall increase in the excitatory charge.

An ultrastructural readout of the average Pr during a fixed number of APs was previously proposed (20–22). The method is based on the assumption that the ratio between exocytosis and endocytosis under 1 Hz stimulation is close to one (22), making it possible to determine, at the ultrastructural level, the number of SVs that fuse in response to each stimulus using extracellular markers such as soluble horseradish peroxidase (HRP). By counting the number of HRP-containing SVs in serial sections of the synaptic terminal, it was possible to estimate the number of SVs that underwent a cycle of exo-endocytosis during a fixed number of APs, yielding an evaluation of the average Pr (Supplementary Material, Fig. S3). In excitatory neurons expressing WT-hSynI, the number of docked SVs (6.0 ± 0.7) and the number of SVs released per AP (0.25 ± 0.04) were highly correlated ($R = 0.79$; $P < 0.001$), as previously reported. On the other hand, excitatory neurons expressing Q555X-hSynI displayed a significantly increased number of docked SVs and a decreased percentage of SVs released by a single AP, consistent with a decreased Pr (Fig. 3H). Inhibitory synapses were characterized by a broader distribution and higher number of SVs released per AP (0.37 ± 0.06 and 0.42 ± 0.05 for Q555X- and WT-hSynI, respectively) and by more numerous docked SVs when compared with excitatory synapses. However, no differences between Q555X- or WT-hSynI positive inhibitory synapses were observed in either the number of docked SVs or the fraction of SVs released by a single AP (Fig. 3G).

Q555X-hSynI differentially alters STP at inhibitory and excitatory synapses

The distinct effects of Q555X-hSynI on the quantal parameters and on the dynamics of release brought us to investigate various forms of STP in Q555X-hSynI expressing neurons such as the responses to paired-pulses or high frequency stimulation (HFS). To study the response to paired-pulse stimulation, synapses were subjected to two consecutive stimuli at interstimulus intervals (ISI) ranging from 25 ms to 2 s. At short ISI (25–50 ms), all Q555X-hSynI expressing synapses displayed an increased response to the second stimulus, resulting in a 3–4-fold enhancement of paired-pulse facilitation (PPF) in excitatory synapses and in a slightly milder paired-pulse depression in inhibitory synapses (Fig. 4A and B). The former effect was reminiscent of the phenotype observed in SynI KO mice (23,24) and is consistent with the decrease in Pr observed with quantal and ultrastructural analyses (see Fig. 3F and H).

Post-tetanic plasticity was studied by applying a stimulation train (1 s at the rate of 40 Hz), followed by single stimulations at 0.1 Hz (Fig. 4C and D). As expected from the different Pr levels, inhibitory synapses expressed post-tetanic depression (PTD), whereas excitatory synapses expressed post-tetanic potentiation (PTP). Interestingly, Q555X-hSynI inhibitory synapses displayed a more intense PTD than WT-hSynI synapses, in the absence of significant changes in the latency after the tetanus (Fig. 4C). On the contrary, Q555X-hSynI excitatory synapses exhibited a significantly larger PTP than WT-hSynI synapses, accompanied by a decrease in latency after the tetanus (Fig. 4D).

Published data indicate that deletion of Syns enhances synaptic depression during sustained HFS, although the effect appears to be more intense at excitatory than at inhibitory synapses (2,5). SynI-transduced neurons were subjected to 30 s HFS to analyze the progressive decay of ePSCs amplitude during the train and the subsequent recovery from depression (Fig. 5A and B). Q555X-hSynI inhibitory synapses showed a lower steady-state current (SSC) during depression, with a significant shortening of the slow time constant of depression. Q555X-hSynI inhibitory synapses also displayed an impaired recovery after depression: the first response after the stimulus train was markedly smaller than in WT-hSynI synapses, and the SSC during recovery was significantly lower (Fig. 5C). This result suggests that Q555X-hSynI impairs SV mobilization during sustained HFS in inhibitory synapses as a consequence of the reduced RP of SVs. In contrast, all depression parameters in Q555X-hSynI excitatory synapses were virtually unchanged, and the recovery kinetics was faster than WT-hSynI synapses, possibly due to a higher SV mobility (25,26) and/or to a more efficient SV recycling (Fig. 5D). These results suggest that the selective impairment of the RP observed in inhibitory synapses can drive an E/I imbalance during prolonged HFS caused by a defective SV mobilization in inhibitory synapses with a substantially preserved excitatory strength.

AZ are shown as mean ± SEM for inhibitory (F) and excitatory (G) synapses expressing either WT-hSynI (black bars) or Q555X-hSynI (open bars). Inhibitory synapses expressing Q555X-hSynI were characterized by a decrease in total SV density attributable to a specific decrease in the pool of SVs more distant from the AZ, whereas the overall SV density and distribution were unchanged in excitatory synapses (inhibitory synapses: $n = 53$ and $n = 55$; excitatory synapses: $n = 50$ and $n = 47$; for WT- and Q555X-hSynI, respectively). (**H** and **I**) The number of SVs physically docked to the AZ was analyzed by serial electron microscopy and three-dimensional reconstructions of the AZ of inhibitory (H) and excitatory (I) synapses expressing either WT-hSynI or Q555X-hSynI. Scale bar, 100 nm. In the lower panels, data are plotted as cumulative distribution of docked SVs per AZ (*left*) and as mean ± SEM (bar plot; *right*). Excitatory synapses displayed an increased number of physically docked SVs ($P < 0.001$, Kolmogorov–Smirnov test versus WT-hSynI distribution), whereas no differences were observed in inhibitory synapses. Inhibitory synapses: $n = 29$ and $n = 39$; excitatory synapses: $n = 20$ and $n = 22$; for WT- and Q555X-hSynI, respectively. $^{*}P < 0.05$; $^{**}P < 0.01$; $^{***}P < 0.001$; Student's *t*-test.

Q555X mutation alters oligomerization of hSynI and its subcellular distribution

Because SV clustering and maintenance of the RP are believed to occur partly through oligomerization of SynI with other Syns (1), we asked whether the Q555X mutation influenced the ability of SynI to oligomerize with other Syn isoforms. To answer this question, we performed co-immunoprecipitation experiments on neurons infected with GFP, WT-hSynI or Q555X-hSynI to test the interaction with SynII isoforms (Fig. 6A). We found that the Q555X truncation virtually abolished the ability of SynI to interact with SynIIa and strongly reduced the interaction with SynIIb. These data indicate that SynI/SynII hetero-oligomerization, which is thought to play an important role in SV clustering, is strongly affected by the mutation.

To assess whether this impaired association of mutant SynI with SynII had any effect on the distribution of Q555X-hSynI in nerve terminals, we performed an ultrastructural analysis by immunogold labeling. As expected, both WT-hSynI and Q555X-hSynI were specifically enriched at presynaptic terminals (Fig. 6B). At rest, the distribution of WT-hSynI was comparable with that reported for the endogenous protein (27) and was characterized by fewer metal particles located near the plasma membrane, when compared with those located in the more central region of the synapse. Interestingly, a 2-fold larger amount of Q555X-hSynI was localized in proximity to the AZ under control conditions, whereas no differences in metal particles were observed in Zones II/III with respect to WT-hSynI (Fig. 6B). When high K^+ stimulation was used to increase intraterminal Ca^{2+},WT-hSynI redistributed more closely to the AZ on stimulation as previously reported (27), whereas the distribution of Q555X-hSynI did not increase further with respect to the resting conditions (Fig. 6C).

The excitatory/inhibitory imbalance in STP increases network hyperexcitability

Increased network excitability is a landmark of epileptogenesis. To address the question of whether changes in STP properties could underlie an increased excitability, we investigated the impact of mutant hSynI on the firing activity and excitability of primary neuronal networks using MEA (4) (Fig. 7A). Under control conditions, Q555X-hSynI-transduced networks exhibited an over 2-fold increase in both firing (Fig. 7B) and bursting (Fig. 7C) rates. To evaluate whether the spontaneous hyperexcitability was associated with impaired inhibition, enhanced excitation or both, network activity was challenged with bicuculline (BIC) to block $GABA_A$ receptors. Interestingly, BIC induced a general and marked increase in both firing and bursting rates (Fig. 7B and C) in WT-hSynI networks, but this effect was greatly attenuated in Q555X-hSynI networks, so that the ratios between BIC and control conditions in Q555X-hSynI were lower than those in WT-hSynI for both spiking and bursting rates (Fig. 7B and C). No differences were observed in burst duration (Fig. 7D) or intra-burst frequency (Fig. 7E) under all conditions analyzed. The spontaneous hyperactivity of Q555X-hSynI networks under basal conditions and the attenuation of the differences between the two experimental groups in the presence of BIC are reminiscent of what was observed in SynI KO cultures (4) and imply that a dynamic impairment of inhibitory transmission plays a fundamental role in the hyperexcitability of Q555X-hSynI networks.

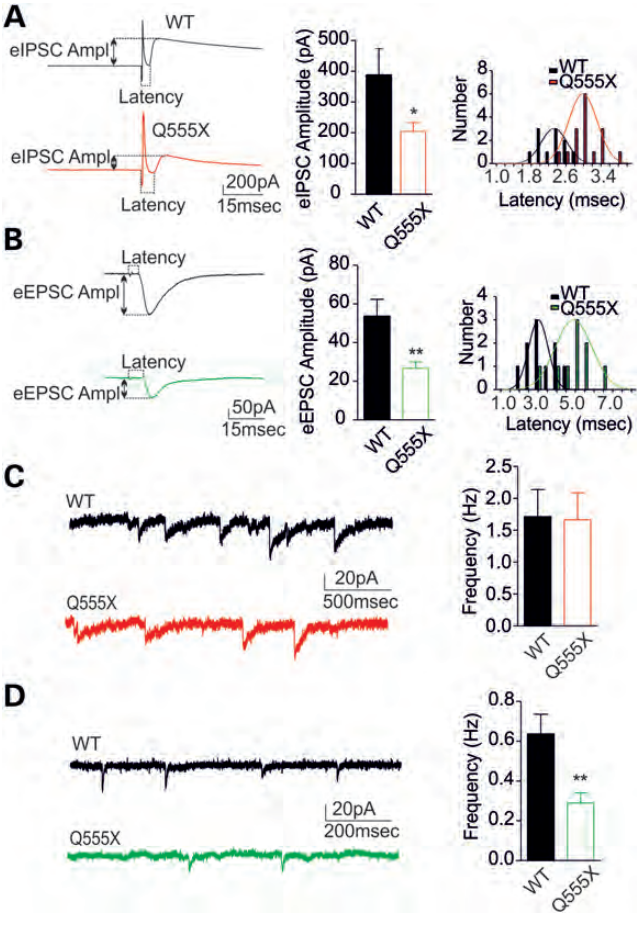

Figure 2. Expression of mutant hSynI decreases the amplitude of both eIPSCs and eEPSCs. (**A** and **B**). Patch-clamp recordings of evoked IPSCs and EPSCs. (*Left*) Averaged traces of eIPSCs (A) and eEPSCs (B) are shown for WT-hSynI (black traces) and Q555X-hSynI (color traces) synapses. (*Center*) Bars indicate the mean (± SEM) amplitude of eIPSCs (A) and eEPSCs (B) recorded in WT-hSynI (black bars) and Q555X-hSynI (color bars) synapses. (*Right*) Frequency distribution of latency times in inhibitory (A) and excitatory (B) synapses expressing either WT-hSynI (black bars) or Q555X-hSynI (color bars). The amplitudes were reduced and the latency times were increased by Q555X-hSynI expression for both eIPSCs and eEPSCs. For further details, see Table 1. Inhibitory synapses: $n = 16$ and $n = 11$; excitatory synapses: $n = 10$ and $n = 11$; for WT- and Q555X-hSynI, respectively. (**C** and **D**). (*Left*) Miniature post-synaptic currents were recorded in inhibitory (C) and excitatory (D) synapses transduced with either WT-hSynI (black traces) or Q555X-hSynI (color traces) in the presence of TTX. (*Right*) The frequencies of mIPSCs and mEPSCs in WT-hSynI (black bars) and Q555X-hSynI (color bars) synapses are reported as mean ± SEM. Inhibitory synapses: $n = 11$ and $n = 8$; excitatory synapses: $n = 17$ and $n = 12$; for WT- and Q555X-hSynI, respectively. $^*P < 0.05$; $^{**}P < 0.01$; Student's *t*-test.

DISCUSSION

In the last few years, several epilepsy and ASD candidate genes involved in synapse development, organization and plasticity have been identified, including genes encoding for

Table 1. Characterization of ePSCs and mPSCs in SynI KO synapses expressing either Q555X-hSynI or WT-hSynI

	hSynI	Amplitude (pA)	Rise time (ms)	Decay time (τ fast; ms)	Decay time (τ slow; ms)	Latency (ms)	CV	*n*
eIPSCs	WT	388.40 ± 85.24	1.66 ± 0.16	20.58 ± 1.70	78.98 ± 7.99	2.27 ± 0.09	0.19 ± 0.04	16
	Q555X	205.0 ± 28.52*	2.07 ± 0.20	21.83 ± 2.70	92.19 ± 11.11	2.98 ± 0.08***	0.26 ± 0.04	11
eEPSCs	WT	53.68 ± 8.71	0.07 ± 0.01	2.68 ± 0.38	19.17 ± 4.10	3.22 ± 0.23	0.27 ± 0.03	10
	Q555X	26.79 ± 3.19**	0.06 ± 0.01	3.14 ± 0.66	14.98 ± 5.69	4.88 ± 0.33***	0.48 ± 0.03***	11
	hSynI	Amplitude (pA)	Rise time (ms)			Decay time (τ; ms)	Frequency (Hz)	*n*
mIPSCs	WT	23.68 ± 0.91	4.16 ± 0.09			29.07 ± 1.20	1.71 ± 0.42	11
	Q555X	24.83 ± 1.36	3.97 ± 0.10			26.74 ± 0.89	1.66 ± 0.43	8
mEPSCs	WT	15.16 ± 0.53	2.04 ± 0.07			4.82 ± 0.31	0.64 ± 0.09	17
	Q555X	14.04 ± 0.51	2.16 ± 0.09			4.98 ± 0.55	0.29 ± 0.05**	12

The amplitude, rise time, decay constants, latency and CV for eIPSCs and eEPSCs as well as amplitude, frequency, rise and decay times for mIPSCs and mEPSCs recorded in SynI KO neurons expressing either WT- or Q555X-hSynI are reported as mean ± SEM.
*$P < 0.05$; **$P < 0.01$, ***$P < 0.001$ Student's *t*-test versus WT-hSynI.

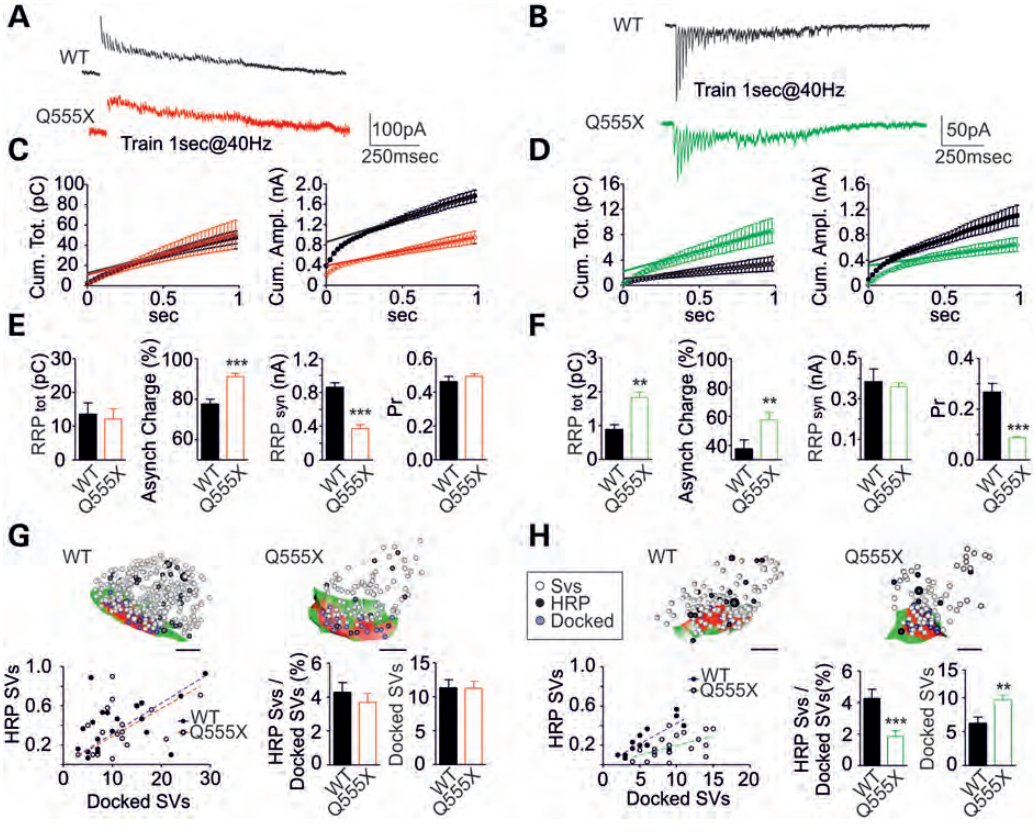

Figure 3. Mutant hSynI decreases synchronous release and increases asynchronous release in both inhibitory and excitatory synapses. (**A**–**D**) A brief stimulation train (1 s at the rate of 40 Hz) was used to study the quantal properties of synchronous and asynchronous release in inhibitory (A) and excitatory (B) synapses transduced with either WT-hSynI (black profiles) or Q555X-hSynI (color profiles). Representative traces are shown. The cumulative curves of eIPSC (C) and eEPSC (D) total charge (in pC; *left*) and amplitude (in nA; *right*) were built, and the linear part was fit as described in the Materials and Methods section. (**E** and **F**) The total charge RRP (RRP_{tot}), the tonic charge transferred during the train (asynchronous charge, expressed in percentage of total charge), the RRP for synchronous release (RRP_{syn}) and release probability (Pr) were deduced from the cumulative curves in C and D and are shown as mean ± SEM for inhibitory (E) and excitatory (F) transmission ($n = 7$). (**G** and **H**) The SV release probability was also estimated by dynamic electron microscopy, by subjecting excitatory and inhibitory neurons to 1 Hz stimulation for 30 s in the presence of extracellular HRP. The number of physically docked SVs and the number of HRP-labeled SVs that underwent fusion were quantified. (*Upper panels*) Three-dimensional reconstructions of inhibitory (G) and excitatory (H) terminals expressing either WT- or Q555X-hSynI are shown. Scale bar, 200 nm. (*Lower panels*) The number of HRP-labeled SVs that underwent fusion in response to a single AP is plotted against the number of physically docked SVs (*left*) for terminals expressing either WT-hSynI (closed circles) or Q555X-hSynI (open circles) and fitted by linear regression [*r* values: 0.49 ($P < 0.05$) and 0.79 ($P < 0.001$) for inhibitory and excitatory synapses expressing WT-hSynI, respectively; slopes ± SEM: 0.028 ± 0.004 and 0.031 ± 0.004 for inhibitory synapses, 0.020 ± 0.002 and 0.040 ± 0.004 for excitatory synapses expressing Q555X- and WT hSynI, respectively]. The percentage of RRP SVs released by a single AP (*middle*) and the number of physically docked SVs (*right*) are shown as mean ± SEM for WT-hSynI (black bars) and Q555X-hSynI (color bars). Inhibitory synapses: $n = 15$ and $n = 15$; excitatory synapses: $n = 9$ and $n = 12$ for WT- and Q555X-hSynI, respectively. **$P < 0.01$; ***$P < 0.001$; Student's *t*-test.

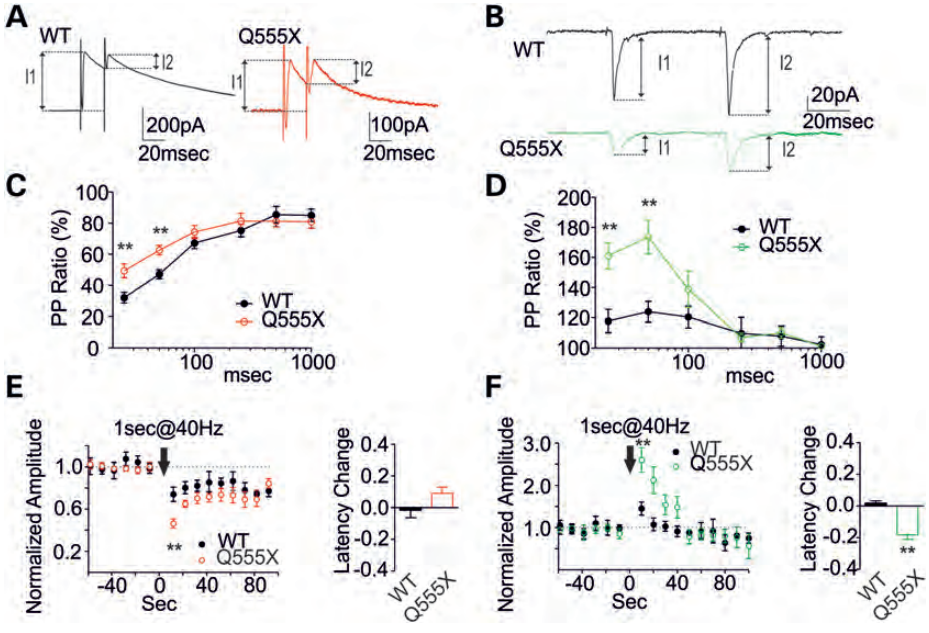

Figure 4. Mutant hSynI induces a marked increase in PPF and PTP in excitatory synapses and a more intense PTD in inhibitory synapses. (**A** and **B**) Paired pulse protocols were applied to inhibitory (A) and excitatory (B) synapses transduced with either WT-hSynI (black profiles) or Q555X-hSynI (color profiles) at ISI ranging from 25 to 1000 ms. The mean ($\pm$ SEM) PPR was calculated and plotted against ISI. Expression of Q555X-hSynI caused an attenuation of paired-pulse depression in inhibitory synapses and a strong enhancement of PPF at short ISI. Inhibitory synapses: $n = 8$ and $n = 14$; excitatory synapses: $n = 10$ and $n = 11$; for WT- and Q555X-hSynI, respectively. (**C** and **D**) The response to a tetanic stimulation (1 s at the rate of 40 Hz) was evaluated in inhibitory (C) and excitatory (D) synapses transduced with either WT-hSynI (black symbols/bars) or Q555X-hSynI (color symbols/bars). The amplitudes of the PSCs recorded after the train as a function of time after the tetanus and normalized to the baseline amplitude (*left*), as well as the relative changes in the latency of the PSCs after the train normalized for the respective baseline latency (*right*), are shown as mean $\pm$ SEM. Inhibitory synapses expressing mutant hSynI display a more pronounced PTD, whereas excitatory synapses expressing mutant hSynI are characterized by an increased PTP and a decreased post-tetanus latency. Inhibitory synapses: $n = 7$ and $n = 8$; excitatory synapses: $n = 6$ and $n = 8$; for WT- and Q555X-hSynI, respectively. $^{**}P < 0.01$; Student's *t*-test.

presynaptic proteins (11,28–31). The recently reported nonsense mutation in exon 12 of SYN1 (32) (C1792T, Q555X) was found in all affected individuals from a large French-Canadian family segregating epilepsy and ASD (14). The implication of SYN1 in epilepsy and ASD was further strengthened by SYN1 missense mutations found in ASD and epileptic patients and by an additional nonsense mutation in exon 9 (G1197A, W356X) identified in a family affected by X-linked syndromic epilepsy that also included one individual affected by aggressive behavior and ASD (33). Both epilepsy and ASD are manifestations of functional abnormalities of cortical circuits and coexist in about 20–30% of patients (34,35). The SYN1 mutations are the first mutations demonstrating that a common genetic defect can be at the basis of both pathologies and that a dysregulation of synaptic homeostasis can play a causal role in the pathogenesis of both diseases.

We studied the physiological effects of the Q555X hSynI mutant by expressing it in primary hippocampal neurons from SynI KO mice. We preferred this experimental system to a human non-neuronal cell line, as such cell lines do not express the complement of presynaptic partners of Syns. In addition, a very high structural and functional conservation exists for the Syn gene family across species (1), and expression of WT-hSynI is able to rescue the developmental and synaptic phenotypes of SynI KO mouse neurons (14). The Q555X mutation studied here maps in the D domain of hSynI, potentially generating a truncated protein that misses about half of the D domain and the COOH-terminal domains E/F for the Ia/Ib splice variants, respectively. Although the premature termination codon of Q555X-hSynI might in principle trigger degradation of the endogenous transcript through nonsense-mediated decay (36), Q555X-hSynI was effectively translated in HeLa cells transfected with either complementary or genomic DNA (Data not shown) and expressed a truncated protein in primary SynI KO neurons that were correctly targeted to nerve terminals, similar to WT-hSynI [see Fig. 1C and Supplementary Material, Fig. S1; (14)]. Although the Q555X-SynI mutant was previously reported to delay axonal growth in early stages of neuronal development *in vitro* (14), no effects were found on the density of excitatory and inhibitory synapses at the later developmental stage used in this paper. This observation fully agrees with the observation that SynI KO neurons display an early delay in axon outgrowth that is eventually caught up at later developmental stages, resulting in a normal synapse density (37).

SynI is not necessary for synaptic transmission, but it regulates synaptic strength through pre- and post-docking actions on SV trafficking that have different impact on excitatory and inhibitory transmission (see 1, for review), similar to what has been described for neuroligins (38). Given the role of SynI in the modulation of release dynamics, we tested whether the Q555X mutation can modify the E/I balance and excitability at the network level by differentially altering basal transmission and/or STP paradigms in excitatory and

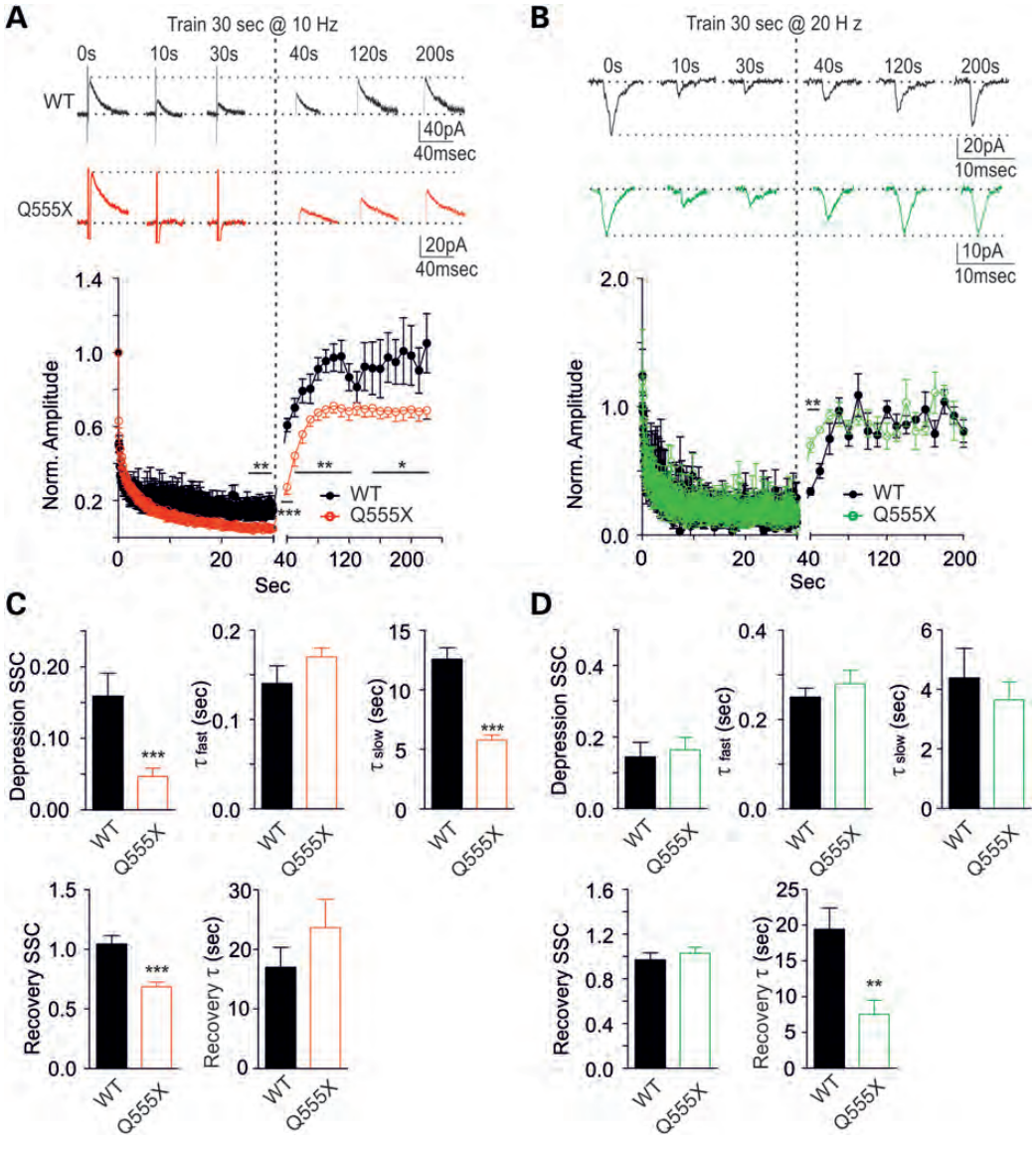

Figure 5. Mutant hSynI increases synaptic depression during sustained HFS in inhibitory synapses. (**A** and **B**) To evaluate synaptic depression, inhibitory (A) and excitatory (B) neurons transduced with either WT-hSynI (black profiles) or Q555X-hSynI (color profiles) were stimulated with trains lasting 30 s at 10 Hz (inhibitory synapses) or 20 Hz (excitatory synapses). (*Upper panels*) Representative traces are shown. (*Lower panels*) The progressive decay of ePSCs amplitude during the stimulation train and the subsequent recovery from depression are plotted (mean ± SEM) as a function of time from the beginning of the train. (**C** and **D**) Depression and recovery in inhibitory (C) and excitatory (D) synapses were individually fitted with bi-exponential (depression) or mono-exponential (recovery) functions to yield time constants (τ) and SSCs after depression and recovery, respectively. The resulting parameters are shown as mean ± SEM in the bar plots. The performance of Q555X-hSynI inhibitory synapses was specifically impaired both during the train and during recovery, whereas Q555X-hSynI excitatory synapses, unaffected during depression, showed faster recovery (inhibitory: $n = 8$ and $n = 13$; excitatory: $n = 8$ and $n = 7$; for WT- and Q555X-hSynI, respectively). $^{*}P < 0.05$; $^{**}P < 0.01$; $^{***}P < 0.001$; Student's *t*-test).

inhibitory synapses. We found that mutant SynI impairs the correct synchronous coupling of SVs to the release machinery, resulting in a decrease in synchronous release and a compensatory enhancement of asynchronous release, particularly intense in excitatory synapses, with a shift of the total transferred charge from inhibitory to excitatory transmission during activity. Despite the similar impairment of evoked synchronous release, quantal analysis and dynamic EM showed that the impairment of evoked synchronous release was caused by a specific decrease in Pr in excitatory synapses and in RRP in inhibitory synapses. While the former effect is likely responsible for the enhancement of PPF and PTP in glutamatergic terminals, the decreased RRP in inhibitory terminals might be the consequence of the overall decrease in SV density and can account for the increased depression. These results underline that, notwithstanding the functional heterogeneity that characterizes excitatory and inhibitory synapses, SynI plays common post-docking actions, favoring a tighter coupling of SVs with the synchronous mechanism of release while restraining asynchronous release.

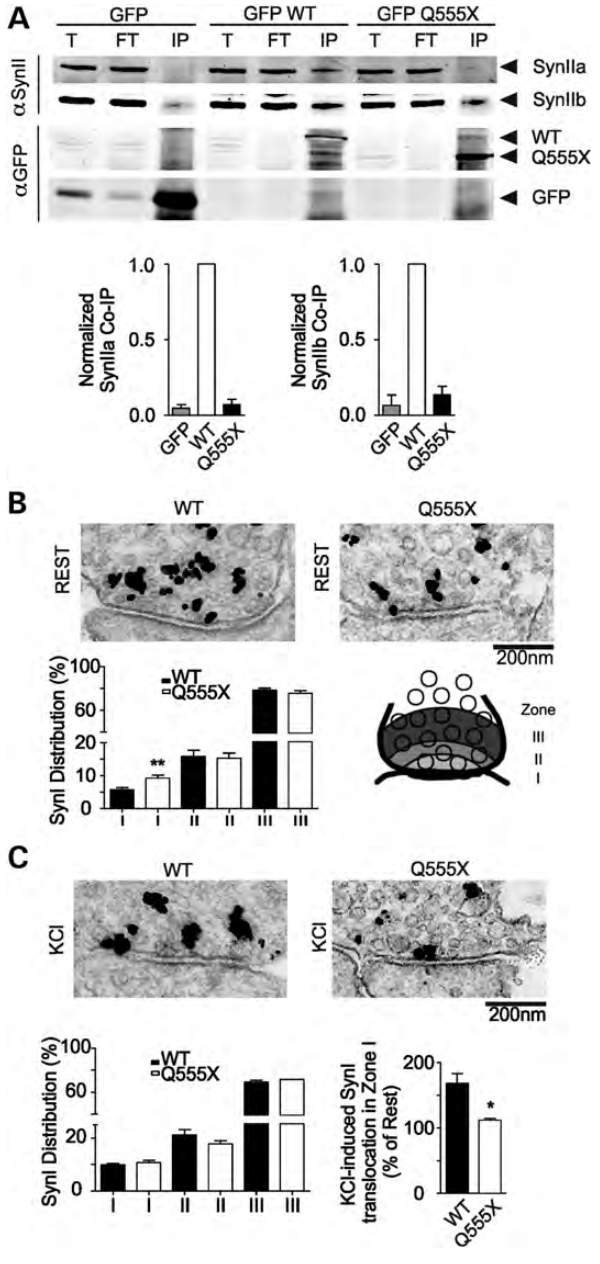

Figure 6. Mutant hSynI displays an impaired association with SynIIa and an altered subcellular distribution in resting nerve terminals. (**A**) Co-immunoprecipitation experiments on neurons infected with GFP, WT-hSynI or Q555X-hSynI were performed to examine whether the Q555X mutation influences the ability of SynI to oligomerize with other Syn isoforms. Primary SynI KO neurons were infected at 6–7 DIV with GFP alone, WT-hSynI or Q555X-hSynI, lysed at 14 DIV and immunoprecipitated with anti-GFP antibodies. After electrophoretic separation of the immunocomplexes, membranes were probed with anti-SynIIa/IIb (αSynII) and anti-GFP (αGFP) antibodies, as indicated. A representative immunoblot is shown in the *upper panel*. In the *lower panel,* SynIIa/IIb immunoreactivity recovered in the IP samples and normalized to the binding of WT-hSynI is shown as mean ± SEM ($n = 3$ experiments performed on neurons derived from three independent litters). T, total lysate (50 μg); FT, flow-through fraction after immunoprecipitation (50 μg); IP, immunoisolated complexes. The Q555X truncation virtually abolished the ability of SynI to interact with both SynII isoforms, indicating that the mutation strongly affects the SynI/SynII hetero-oligomerization that is thought to play an important role in SV clustering. (**B**) Ultrastructural analysis by immunogold labeling revealed an enrichment of both WT-hSynI (closed bars) and Q555X-hSynI (open bars) at presynaptic terminals. Synapses were divided into three radial areas (I, II and III) from the AZ to the distal RP area, and the density of the immunogold particles was calculated and shown as mean ± SEM ($n = 93$ and $n = 90$ synapses for WT-hSynI and Q555X-hSynI from three independent experiments). At rest, the distribution of WT-hSynI was comparable with that reported for the endogenous protein (27) and was characterized by fewer metal particles located near the plasma membrane, when compared with those located in the more central region of the synapse. Interestingly, a 2-fold larger amount of Q555X-hSynI was localized in proximity to the AZ under control conditions, whereas no differences in metal particles were observed in Zones II/III with respect to WT-hSynI. $^{**}P < 0.01$; ANOVA for repeated measures (mean gold particle density/synapse: 10.76 ± 0.69 and 8.38 ± 0.53 for WT- and Q555X-hSynI, respectively; 1.15 ± 0.15 negative control in the absence of primary antibody). (**C**) Depolarization with high K^+ (56 mM) was used to increase intraterminal Ca^{2+} and to follow the redistribution of WT- and mutant hSynI at the ultrastructural level ($n = 87$ and $n = 89$ synapses for WT-hSynI and Q555X-hSynI from $n = 3$ independent experiments; *left*). The depolarization-dependent translocation of WT-hSynI and Q555X-hSynI into Zone I, calculated in percentage of the respective density of immunogold particles under resting conditions, is plotted as mean ± SEM (*right*). Whereas WT-SynI was translocated toward the AZ (Zone I) in response to depolarization as previously reported (27), the distribution of Q555X-hSynI did not further increase with respect to the resting conditions. $^{*}P < 0.05$; $^{**}P < 0.01$; Student's *t*-test.

Despite similar effects on basal transmission, STP of excitatory and inhibitory synapses was affected in opposite directions by the SynI mutation. Indeed, excitatory synapses expressing mutant SynI showed markedly increased PPF, PTP and faster recovery from depression, but no change in synaptic depression extent and dynamics. On the contrary, inhibitory synapses displayed an enhancement of synaptic depression in response to both short and sustained HFS, with a marked slow down of the recovery from depression. The opposite effects of the SynI mutant on excitatory and inhibitory STP support the idea that an E/I imbalance in the STP domain might potentially underlie a state of hyperexcitability in neuronal networks expressing the mutant protein. Indeed, the analysis of the activity of neuronal networks expressing Q555X-SynI showed a clear-cut increase in both firing and bursting activities. Such increased excitability was largely dependent on the impairment of inhibitory synaptic transmission as shown by the scarce effects of the $GABA_A$ receptor blockade on the firing and bursting rates. This indicates that: (i) impairments in inhibitory transmission are more important in shaping network excitability than primary changes in excitatory transmission and (ii) network dynamics and excitability are highly dependent on STP dynamics of excitatory and inhibitory synapses rather than on their basal transmission properties.

It was of interest to compare the Q555X phenotype with that of SynI deletion to establish the extent to which the Q555X mutant of hSynI mimics the SynIKO phenotype. A detailed comparison of the electrophysiological and morphological phenotypes observed after expression of Q555X-SynI in SynI KO neurons with the corresponding phenotypes observed after deletion of SynI (Table 2) reveals that the Q555X mutant of hSynI fully phenocopies the mouse SynI KO phenotype in inhibitory neurons. As the data indicate that the inhibitory impairment is likely to be the primum movens in the SynI-linked epileptogenesis [(4); see Fig. 7], this conforms to a loss-of-function character of the Q555X mutation. However, in excitatory neurons, the mutant does not fully phenocopy the mouse SynI KO phenotype. Although it mimics the KO

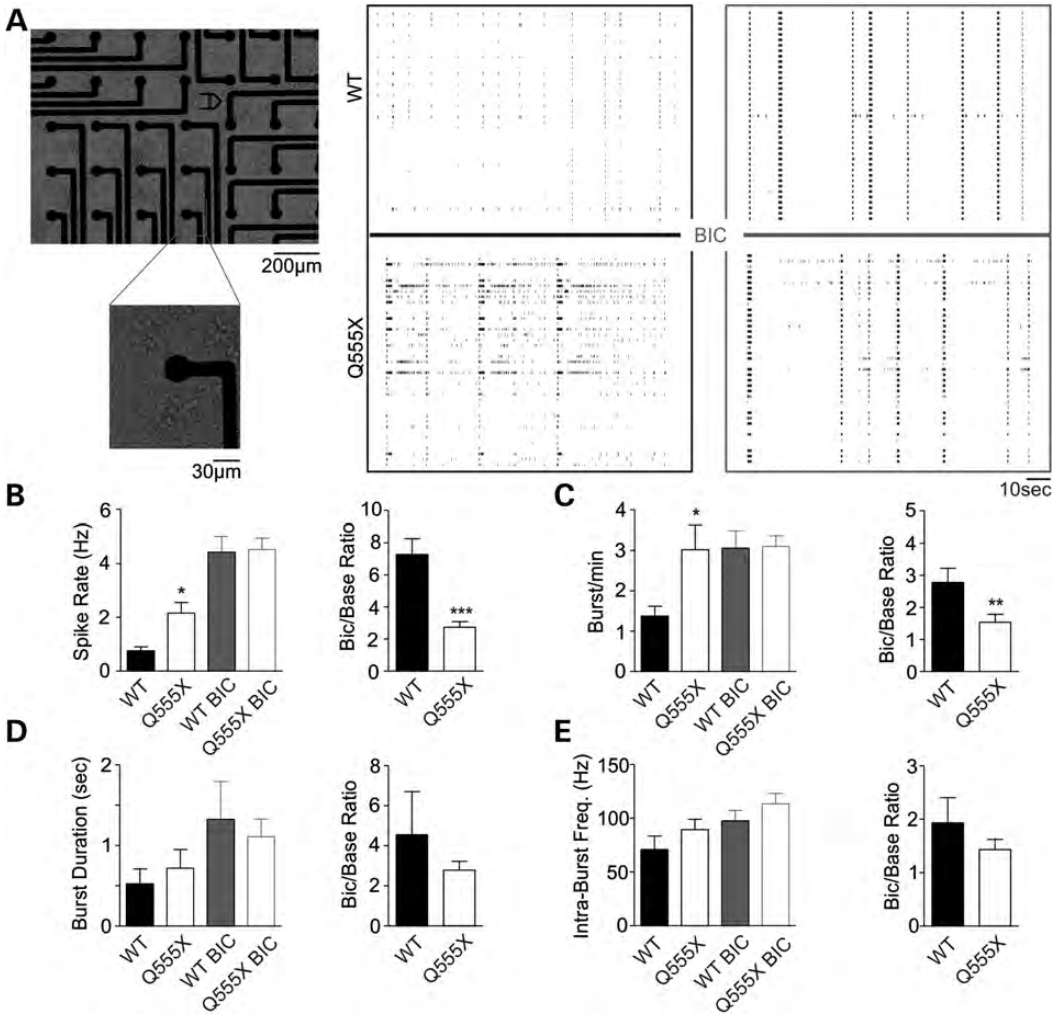

Figure 7. Primary networks expressing mutant hSynI become hyperexcitable. (**A**) Primary SynI KO hippocampal neurons were grown onto MEA chips and transduced to express either WT-hSynI or Q555X-hSynI. A representative microphotograph of neurons on MEA (*left*) and representative raster plots of spontaneous activity at 20 DIV (*right*) showing spiking and bursting activities are shown.(**B**–**E**) Spike rate (B), burst rate (C), burst duration (D) and intra-burst spike frequency (E) were measured from the raster plots of spontaneous activity and are plotted (*left panels*) as mean ± SEM for WT-hSynI ($n = 12$; closed bars) or Q555X-hSynI ($n = 19$; open bars) networks under basal conditions (black bars) or in the presence of BIC (gray bars). A significant increase in excitability, evaluated as spike and burst rates, was present in Q555X-hSynI networks with respect to WT-hSynI networks under basal conditions. These differences, however, virtually disappeared in the presence of BIC, with a more dramatic effect of the $GABA_A$ block in WT-hSynI networks than in Q555X-hSynI ones. The ratio between the individual values of each network parameter under BIC and basal conditions (BIC/base ratio) is plotted as mean ± SEM (*right panels*). $^{*}P < 0.05$; $^{**}P < 0.01$; $^{***}P < 0.001$; Student's *t*-test.

phenotype in STP paradigms such as PPF and depression, it induces a decrease in release probability that may represent a specific gain-of-function of the mutant. This effect on release probability is likely responsible for the decreases in eEPSC amplitude and mEPSC frequency as well as for the increased number of docked SVs, all effects that are not detected in SynI KO neurons [Table 2 and Supplementary Material, Fig. S4; (3,4,23,24,39–43)].

What could be the basis of the loss-of-function of the Q555X hSynI mutant? In addition to the previously shown impairments in the interactions with Src, CaMKII and Erk (14), we have found that, in co-immunoprecipitation assays, mutant hSynI is virtually unable to interact with SynIIa/IIb. This finding, therefore, underlines the importance of domain E present in Syns Ia and IIa and of its synergistic interaction with the central domain C, in mediating the SynI/SynII interactions as well as in regulating the maintenance of the RP and the post-docking steps of release (15,44). As Syn oligomerization is thought to play an important role in SV clustering (15,44–46), the impairment of SynI/SynII heterodimerization may result in an altered distribution of mutant SynI within nerve terminals. As a matter of fact, immunogold labeling at rest revealed a 2-fold higher amount of Q555X-hSynI close to the AZ with respect to WT-hSynI that did not further increase in response to depolarization. These data indicate that the Q555X mutation profoundly alters the subcellular distribution and the molecular interactions of SynI, with a potential impact in SV trafficking.

In this work, we show that the Q555X hSynI mutation affects excitatory and inhibitory transmission leading to E/I

Table 2. Comparison of the SynI KO and Q555X-SynI phenotypes

Phenotype	SynI KO		Q555X-SynI	
	Inhibitory neurons	Excitatory neurons	Inhibitory neurons	Excitatory neurons
Basal transmission				
mPSC frequency	= (3,4)	= (4)	=	↓
ePSC amplitude	↓ (3,4)	↑ (4)	↓	↓
RRPsynch	↓ (3,4)	↑ (4)	↓	=
RRPasynch	↑ (43)	nd	↑	↑
Pr	= (3,4)	= (4)	=	↓
STP				
Paired pulse	= (3,4)	↑ (4,23,24)	≈	↑
Post-tetanus	= (3)	≈/↓(24,42)	≈	↑
Depression	↑ (3)	= (ud)	↑	=
SV density				
Total pool	↓ (41, §)	↓ (39,40, §)	↓	=
Docked pool	= (§)	= (§)	=	↑

The effects of SynI deletion (SynI KO) on the quantal parameters of basal release, STP paradigms and SV density in the distal and proximal pools are compared with a summary of the effects on the Q555X-SynI mutant expressed in SynI KO neurons. Reference to published papers are reported in parenthesis. (nd, not determined; ud, F. Benfenati *et al*., unpublished data. Symbols: ↓, decrease; ↑, increase; =, no effect; ≈, mild effect; §, Supplementary Material, Fig. S4).

imbalance and network hyperexcitability. Our data are consistent with the idea that altered E/I balance and impairment of GABAergic systems are landmarks of numerous neuropsychological disorders, including epilepsy and ASD (7,8,47). From a more physiological perspective, our results emphasize the key role of STP of excitatory and inhibitory synapses in shaping network dynamics, consistent with the filtering, integration and pattern detection activities operated by STP in neural networks (48).

MATERIALS AND METHODS

Materials

The following primary antibodies were used: monoclonal anti-SynIIa/IIb (clone 19.21), monoclonal anti-Src (clone 327, Sigma-Aldrich, Milano, Italy) and polyclonal anti-GFP (A11122, Invitrogen, Monza, Italy). VGAT and VGLUT1 (Synaptic System, Gottingen, Germany). Amino-5-phosphonopentanoic acid (D-AP5), 6-cyano-7-nitroquinoxaline-2,3-dione (CNQX), CGP58845 BIC and tetrodotoxin (TTX) were from Tocris (Bristol, UK). Cell culture media were from Invitrogen. All other chemicals were from Sigma.

Primary cultures of SynI KO hippocampal neurons

SynI KO mice were generated by homologous recombination (37). All experiments were carried out in accordance with the guidelines established by the European Community Council (Directive 2010/63/EU of September 22, 2010) and were approved by the Italian Ministry of Health. Pregnant females were killed by inhalation of CO_2, and embryonic day 17 embryos were removed immediately by Cesarean section. Isolated hippocampal neurons were plated at low density [20 cells/mm^2; (3)] and maintained in a culture medium consisting of Neurobasal, B-27 (1:50 v/v), glutamax (1% w/v) and penicillin–streptomycin (1%).

Virus production and neuron transduction

Sequences containing EGFP-WT-hSynIa and EGFP-Q555X-hSynIa were cloned into pLenti6.2/V5-Dest plasmids (Invitrogen). The production of VSV-pseudotyped third-generation lentiviruses was performed as previously described (49). Viral titers ranging from 1.0 to 5.0 $\times$ 10^8 TU/ml were obtained for both WT-hSynI and Q555X-hSynI vectors. Primary hippocampal neurons were infected at six to 7 DIV at 10 multiplicity of infection. After 24 h, half of the medium was replaced with fresh medium. All experiments were performed between 12 and 18 DIV. The expression levels of WT- and Q555X-hSynI were assessed by GFP fluorescence.

Patch-clamp recordings

Patch electrodes, fabricated from thick borosilicate glass (Hilgenberg, Mansfield, Germany), were pulled and fire polished to a final resistance of 5–7 MΩ. Whole-cell patch-clamp recordings from post-synaptic neurons were performed using an Axon Multiclamp 700B/Digidata1440A system (Molecular Devices, Sunnyvale, CA, USA) and an upright BX51WI microscope (Olympus, Tokyo, Japan) equipped with Nomarski optics. Experiments were performed on 12–18 DIV neurons using an extracellular electrode to stimulate release from the presynaptic compartment of infected neurons in inhibitory synapses and dual patch clamp in excitatory synapses. ePSCs were recorded in extracellular solution (Tyrode solution) containing (in mM): 2 $CaCl_2$, 140 NaCl, 1 $MgCl_2$, 10 HEPES, 4 KCl and 10 glucose, pH 7.3. For inhibitory transmission, D-AP5 (50 μM), CNQX (10 μM) and CGP58845 (5 μM) were added to block NMDA, non-NMDA and $GABA_B$ receptors, respectively. For excitatory transmission, D-AP5 (50 μM) and BIC (30 μM) were added to block NMDA and $GABA_A$ receptors, respectively. Miniature PSCs were recorded with TTX (300 nM) in the extracellular solution. The size of the RRP of synchronous release (RRP_{syn}) and the probability that any given SV in the RRP will be released (Pr) were calculated using the cumulative amplitude analysis (50).

RRP_{syn} was determined by summing up peak PSC amplitudes during 40 repetitive stimuli applied at 40 Hz. The cumulative amplitude profiles of the last 15–20 data points were fitted by linear regression and back extrapolated to time 0. The intercept with the *Y*-axis gave the RRP_{syn} and the ratio between the amplitude of the first ePSC (I_1) and RRP yielded the Pr. Asynchronous release was evaluated, for each response in train, as the difference between the total transferred charge and the synchronous charge. The synchronous charge component of each response was calculated as the integral of the current with respect to an individual baseline determined 2 ms before each stimulus (18,19), using a proprietary program developed in an R-CRAN environment. The total release during the train was calculated using cumulative charge analysis in the same way of cumulative amplitude analysis, to include in the analysis synchronous and asynchronous release components (51). To study the response to paired-pulse protocols, we applied two consecutive stimuli at increasing interpulse intervals (25–1000 ms). To analyze PTD and PTP, we applied a stimulus every 10 s after the tetanus (1 s at the rate of 40 Hz) and normalized the PSC amplitude to the baseline.

MEA recordings

Dissociated hippocampal neurons were plated onto a planar Muse MultiElectrode Array (Axion Biosystems, Atlanta, GA, USA). The electrode diameter was 30 μm, and the orthogonal distances between electrodes were 200 μm. The day before dissociation, the active electrode area was coated overnight with poly-D-lysine (0.1 mg/ml). On the day of the preparation, poly-D-lysine was substituted with a small drop (75 μl) of laminin (5 μl/ml, Sigma-Aldrich) diluted in Neurobasal. The Muse 64 channel amplifier (gain 1200, 61 dB) connected to an external hardware controller via a National Instrument analog-to-digital card was used to amplify extracellular raw data. Raw data were digitized at 20 kHz and stored on a hard disk for off-line analysis. Spike detection of single extracellular APs was performed using the Axion Biosystem software using a voltage threshold of six times the standard deviation of the noise over 200 Hz high-pass filtered traces. Spike train data were analyzed using the Neuroexplorer software (Plexon, Dallas, TX, USA). Bursts were detected using the burst analysis algorithm of Neuroexplorer with the following criteria: maximum inter-spike interval 200 ms, minimum burst duration 20 ms and minimum number of spikes per burst five. Cultures were recorded between 18 and 21 DIV under control conditions (substituting Neurobasal with Tyrode solution) in the MEA chamber maintained at 36.5°C for at least 30 min. Then, BIC (30 μM) was applied to the bath, and the recording was continued for further 30 min.

Immunofluorescence

Primary hippocampal neurons were fixed with 4% paraformaldehyde, 4% sucrose in 0.12 M phosphate buffer, pH 7.4, rinsed several times in phosphate-buffered saline (PBS), blocked and permeabilized in 0.1% gelatin, 0.3% Triton X-100 in PBS. Samples were sequentially incubated with primary antibodies and fluorochrome-conjugated secondary antibodies (Invitrogen). After several washes in PBS, coverslips were mounted using Prolong Gold antifade reagent (Invitrogen). For quantification of the number of inhibitory and excitatory synapses, cultured neurons were stained for VGAT (1:500 dilution) and VGLUT1 (1:200 dilution). Images were acquired using a DS-Ri1 camera on an Eclipse 80i microscope equipped with a Planfluor 40×/0.75 objective (Nikon Instruments, Amstelveen, The Netherlands). The percentage of fluorescent VGAT or VGLUT1 puncta was automatically counted using the MetaMorph Count Nuclei application module (Molecular Devices). For the quantification of GFP fluorescence intensity, cultured neurons were stained with anti-GFP antibody (1:1000; Invitrogen). Digital images were acquired as above, and GFP intensity in the images was calculated using ImageJ after subtracting a threshold level of fluorescence. To quantify GFP intensity in inhibitory and excitatory synapses, cultured neurons co-stained for GFP, VGAT and VGLUT1 were acquired using a 63× objective in a Leica SP5 confocal. The intensity of the GFP signal colocalizing with VGAT or VGLUT1, respectively, was quantified using the JACOP plugin of ImageJ (52). The density of puncta was calculated as the number of vGLUT1- or vGAT-positive puncta per square micrometer.

Electron microscopy

For conventional transmission electron microscopy, primary cortical neurons were fixed with 1.3% glutaraldehyde in 66 mM sodium cacodylate buffer, post-fixed in 1% OsO_4, 1.5% $K_4Fe(CN)_6$, 0.1 M sodium cacodylate, *en bloc* stained with 0.5% uranyl acetate, dehydrated and embedded in Epon. Ultrathin sections were contrasted with 2% uranyl acetate and Sato's lead solution, observed with a JEM-1011 microscope (Jeol, Tokyo, Japan) at 100 kV and imaged with an ORIUS SC1000 CCD camera (Gatan, Pleasanton, CA, USA). Synapses were divided into two groups according to their ultrastructural features: excitatory (asymmetric) synapses were distinguished by the presence of a thickened post-synaptic density, whereas inhibitory (symmetric) synapses were selected for the presence of pre- and post-synaptic membranes more parallel than the surrounding non-synaptic membrane and the absence of a prominent post-synaptic density. Synaptic area, SV number and distance from the AZ were quantified using the Image J software. For HRP uptake, hippocampal neurons were infected at seven DIV with EGFP-WT-hSynI or EGFP-Q555X-hSynI. Neurons were electrically stimulated at 14 DIV in the presence of 10 μM CNQX/50 μM AP5 and 10 mg/ml HRP by applying field 1 ms current pulses of 20 μA at 1 Hz for 30 s with an isolated pulse stimulator (AM-System M2100, X). Neurons were then washed, fixed with 1.3% glutaraldehyde in 66 mM sodium cacodylate buffer, incubated with 0.3 mg/ml 3′,3′-diaminobenzidine/0.03% H_2O_2 up to 30 min and further processed for conventional TEM preparation. Serial 60 nm sections were collected on carbon-coated formvar grids and imaged as described above. Synapses in which the AZ was clearly visible throughout the serial sections were imaged and the total numbers of HRP-positive and docked SVs were calculated. Pre-embedding immunogold electron microscopy was carried out

as previously described (27). Briefly, cultured neurons were fixed with 4% paraformaldehyde in 0.1 M phosphate buffer, pH 7.4 for 1 h at room temperature. After several washes in PBS, coverslips were permeabilized in 5% normal goat serum/0.1% saponin in PBS for 1 h and incubated with rabbit anti-GFP (1:500 dilution) for 2 h. After several washes in 1% normal goat serum/0.1 saponin in PBS, neurons were incubated with 1.4 nm NANOGOLD Fab' fragment of goat anti-rabbit (1:100 dilution; Invitrogen), washed and fixed in 1.25% glutaraldehyde in PBS. NANOGOLD was amplified using silver enhancement (LI silver enhancement, Invitrogen) and neurons were treated with 0.2% OsO_4 for 30 min, 0.25% uranyl acetate overnight, dehydrated in ethanol and embedded in Epon. Due to the mild fixation used in the immunolabeling procedure, it was not always possible to unambiguously discriminate between symmetric and asymmetric synapses. Therefore, all synapse types were included in this analysis. The distances from the center of metal particles and the AZ were measured with the Image J software.

Immunoprecipitation

Primary neurons from SynI KO embryos were infected with GFP, GFP-WT-hSynI or GFP-Q555X-hSynI as described above. Cells were washed once in ice-cold PBS and lysed in RIPA buffer (50 mM Tris–HCl pH 7.4, 150 mM NaCl, 2 mM EDTA, NP40 1% and SDS 0.1%) plus protease inhibitors (complete EDTA-free protease inhibitors, Roche Diagnostic, IN, USA) for 30 min at 4°C under constant agitation. After centrifugation at 16 000*g* for 15 min at 4°C, protein concentration in the extract was quantified using the Bradford Protein Assay (BioRad, Segrate, Italy). Following protein extraction, lysates were precleared using 25 µl Protein A Sepharose Fast Flow (GE Healthcare, Milano, Italy) for 1 h at 4°C. Precleared lysates were incubated overnight at 4°C with 3 µg of GFP antibodies, and the immunocomplexes were then isolated by adding Protein A Sepharose for 2 h at 4°C. SDS-PAGE and western blotting were performed using precast 10% NuPAGE® Novex® Bis-Tris Gels (Invitrogen). After incubation with primary antibodies, membranes were incubated with fluorescently conjugated secondary antibodies (ECL Plex™ goat α-rabbit IgG-Cy5 and ECL Plex™ goat α-mouse IgG-Cy3; GE Healthcare) and revealed by a Typhoon TRIO+ Variable Mode Imager (GE Healthcare).

Statistical analysis

Data were analyzed by paired/unpaired Student's *t*-test or, in case of more than two experimental groups, by one-way ANOVA followed by *post-hoc* multiple comparison tests using the SPSS software (SPSS, Inc., Chicago, IL, USA). Significance level was preset to $P < 0.05$. Data are expressed as means ± SEM for number of cells (*n*). The normal distribution of experimental data was assessed using the Kolmogorov–Smirnov test.

SUPPLEMENTARY MATERIAL

Supplementary Material is available at *HMG* online.

ACKNOWLEDGEMENTS

We thank Drs Hung-Teh Kao (Brown University, Providence, RI, USA) and Paul Greengard (The Rockefeller University, New York, NY, USA) for providing us with the SynI KO mouse strain; Drs Luigi Naldini and Mario Amendola (Tigem, Milano, Italy) for invaluable help in lentiviral production protocols; Axion Biosystems (Atlanta, GA, USA) for collaboration in testing the Muse System; Marina Nanni (Istituto Italiano di Tecnologia, Genova, Italy) for precious help with cell cultures and Drs Anna Fassio (University of Genova, Italy), Lucian Medrihan, Joachim Scholz-Starke and Thierry Nieus (Istituto Italiano di Tecnologia, Genova, Italy) for useful discussions.

Conflict of Interest statement. None declared.

FUNDING

This work was supported by research grants from the Italian Ministry of University and Research (PRIN to P.B. and F.B.), the Italian Ministry of Health Progetto Giovani (to P.B.), the Compagnia di San Paolo, Torino (to P.B. and F.B.) and the Quebec Ministry of International Relationships and Italian Ministry of Foreign Affairs (to P.C. and F.B.). The support of Telethon-Italy (Grant GGP09066 to P.B., GGP09134 to F.B. and F.V.) and European Union's FP7/2007-2013 grant "FOCUS" are also acknowledged. Funding to pay the Open Access publication charges for this article was provided by Telethon - Italy.

REFERENCES

1. Cesca, F., Baldelli, P., Valtorta, F. and Benfenati, F. (2010) The synapsins: key actors of synapse function and plasticity. *Prog. Neurobiol.*, **91**, 313–348.
2. Gitler, D., Takagishi, Y., Feng, J., Ren, Y., Rodriguiz, R.M., Wetsel, W.C., Greengard, P. and Augustine, G.J. (2004) Different presynaptic roles of synapsins at excitatory and inhibitory synapses. *J. Neurosci.*, **24**, 11368–11380.
3. Baldelli, P., Fassio, A., Valtorta, F. and Benfenati, F. (2007) Lack of synapsin I reduces the readily releasable pool of synaptic vesicles at central inhibitory synapses. *J. Neurosci.*, **27**, 13520–13531.
4. Chiappalone, M., Casagrande, S., Tedesco, M., Valtorta, F., Baldelli, P., Martinoia, S. and Benfenati, F. (2009) Opposite changes in glutamatergic and GABAergic transmission underlie the diffuse hyperexcitability of synapsin I-deficient cortical networks. *Cereb. Cortex*, **19**, 1422–1439.
5. Farisello, P., Boido, D., Nieus, T., Medrihan, L., Cesca, F., Valtorta, F., Baldelli, P. and Benfenati, F. (2012) Synaptic and extrasynaptic origin of the excitation/inhibition imbalance in the hippocampus of synapsin I/II/III knockout mice. *Cereb. Cortex*, **23**, 581–593.
6. Boido, D., Farisello, P., Cesca, F., Ferrea, E., Valtorta, F., Benfenati, F. and Baldelli, P. (2010) Cortico-hippocampal hyperexcitability in synapsin I/II/III knockout mice: age-dependency and response to the antiepileptic drug levetiracetam. *Neuroscience*, **171**, 268–283.
7. Chao, H.-T., Chen, H., Samaco, R.C., Xue, M., Chahrour, M., Yoo, J., Neul, J.L., Gong, S., Lu, H.-C., Heintz, N. *et al.* (2010) Dysfunction in GABA signalling mediates autism-like stereotypies and Rett syndrome phenotypes. *Nature*, **468**, 263–269.
8. Bradford, H.F. (1995) Glutamate, GABA and epilepsy. *Prog. Neurobiol.*, **47**, 477–511.
9. Cobos, I., Calcagnotto, M.E., Vilaythong, A.J., Thwin, M.T., Noebels, J.L., Baraban, S.C. and Rubenstein, J.L. (2005) Mice lacking Dlx1 show subtype-specific loss of interneurons, reduced inhibition and epilepsy. *Nat. Neurosci.*, **8**, 1059–1068.

10. Eichler, S.A. and Meier, J.C. (2008) E-I balance and human diseases – from molecules to networking. *Front. Mol. Neurosci.*, **1**, 2.
11. Jamain, S., Quach, H., Betancur, C., Råstam, M., Colineaux, C., Gillberg, I.C., Soderstrom, H., Giros, B., Leboyer, M., Gillberg, C. *et al.* (2003) Mutations of the X-linked genes encoding neuroligins NLGN3 and NLGN4 are associated with autism. *Nat. Genet.*, **34**, 27–29.
12. Greco, B., Manago, F., Tucci, V., Kao, H.T., Valtorta, F. and Benfenati, F. (2012) Autism-related behavioral abnormalities in synapsin knockout mice. *Behav. Brain. Res*. doi: 10.1016/j.bbr.2012.12.015.
13. Corradi, A., Zanardi, A., Giacomini, C., Onofri, F., Valtorta, F., Zoli, M. and Benfenati, F. (2008) Synapsin-I- and synapsin-II-null mice display an increased age-dependent cognitive impairment. *J. Cell Sci.*, **121**, 3042–3051.
14. Fassio, A., Patry, L.e., Congia, S., Onofri, F., Piton, A., Gauthier, J., Pozzi, D., Messa, M., Defranchi, E., Fadda, M. *et al.* (2011) SYN1 loss-of-function mutations in autism and partial epilepsy cause impaired synaptic function. *Hum. Mol. Genet.*, **20**, 2297–2307.
15. Hilfiker, S., Pieribone, V.A., Czernik, A.J., Kao, H.T., Augustine, G.J. and Greengard, P. (1999) Synapsins as regulators of neurotransmitter release. *Philos. Trans. R. Soc. Lond. B Biol. Sci.*, **354**, 269–279.
16. Humeau, Y., Doussau, F., Vitiello, F., Greengard, P., Benfenati, F. and Poulain, B. (2001) Synapsin controls both reserve and releasable synaptic vesicle pools during neuronal activity and short-term plasticity in Aplysia. *J. Neurosci.*, **21**, 4195–4206.
17. Goda, Y. and Stevens, C.F. (1994) Two components of transmitter release at a central synapse. *Proc. Natl. Acad. Sci. USA*, **91**, 12942–12946.
18. Otsu, Y. and Murphy, T.H. (2004) Optical postsynaptic measurement of vesicle release rates for hippocampal synapses undergoing asynchronous release during train stimulation. *J. Neurosci.*, **24**, 9076–9086.
19. Yao, J., Gaffaney, J.D., Kwon, S.E. and Chapman, E.R. (2011) Doc2 is a Ca2+ sensor required for asynchronous neurotransmitter release. *Cell*, **147**, 666–677.
20. Branco, T., Staras, K., Darcy, K.J. and Goda, Y. (2008) Local dendritic activity sets release probability at hippocampal synapses. *Neuron*, **59**, 475–485.
21. Branco, T., Marra, V. and Staras, K. (2010) Examining size-strength relationships at hippocampal synapses using an ultrastructural measurement of synaptic release probability. *J. Struct. Biol.*, **172**, 203–210.
22. Fernández-Alfonso, T. and Ryan, T.A. (2004) The kinetics of synaptic vesicle pool depletion at CNS synaptic terminals. *Neuron*, **41**, 943–953.
23. Rosahl, T.W., Geppert, M., Spillane, D., Herz, J., Hammer, R.E., Malenka, R.C. and Südhof, T.C. (1993) Short-term synaptic plasticity is altered in mice lacking synapsin I. *Cell*, **75**, 661–670.
24. Rosahl, T.W., Spillane, D., Missler, M., Herz, J., Selig, D.K., Wolff, J.R., Hammer, R.E., Malenka, R.C. and Südhof, T.C. (1995) Essential functions of synapsins I and II in synaptic vesicle regulation. *Nature*, **375**, 488–493.
25. Fornasiero, E.F., Raimondi, A., Guarnieri, F.C., Orlando, M., Fesce, R., Benfenati, F. and Valtorta, F. (2012) Synapsins contribute to the dynamic spatial organization of synaptic vesicles in an activity-dependent manner. *J. Neurosci.*, **32**, 12214–12227.
26. Orenbuch, A., Shalev, L., Marra, V., Sinai, I., Lavy, Y., Kahn, J., Burden, J.J., Staras, K. and Gitler, D. (2012) Synapsin selectively controls the mobility of resting pool vesicles at hippocampal terminals. *J. Neurosci.*, **32**, 3969–3980.
27. Tao-Cheng, J.-H. (2006) Activity-related redistribution of presynaptic proteins at the active zone. *Neuroscience*, **141**, 1217–1224.
28. Kumar, A., Sundaram, S.K., Sivaswamy, L., Behen, M.E., Makki, M.I., Ager, J., Janisse, J., Chugani, H.T. and Chugani, D.C. (2010) Alterations in frontal lobe tracts and corpus callosum in young children with autism spectrum disorder. *Cereb. Cortex*, **20**, 2103–2113.
29. Laumonnier, F., Bonnet-Brilhault, F., Gomot, M., Blanc, R., David, A., Moizard, M.-P., Raynaud, M., Ronce, N., Lemonnier, E., Calvas, P. *et al.* (2004) X-linked mental retardation and autism are associated with a mutation in the NLGN4 gene, a member of the neuroligin family. *Am. J. Hum. Genet.*, **74**, 552–557.
30. Pavlowsky, A., Gianfelice, A., Pallotto, M., Zanchi, A., Vara, H., Khelfaoui, M., Valnegri, P., Rezai, X., Bassani, S., Brambilla, D. *et al.* (2010) A postsynaptic signaling pathway that may account for the cognitive defect due to IL1RAPL1 mutation. *Curr. Biol.*, **20**, 103–115.
31. Piton, A., Michaud, J.L., Peng, H., Aradhya, S., Gauthier, J., Mottron, L., Champagne, N., Lafrenière, R.G., Hamdan, F.F., Team, SD *et al.* (2008) Mutations in the calcium-related gene IL1RAPL1 are associated with autism. *Hum. Mol. Genet.*, **17**, 3965–3974.
32. Sudhof, T.C. (1990) The structure of the human synapsin I gene and protein. *J. Biol. Chem.*, **265**, 7849–7852.
33. Garcia, C.C., Blair, H.J., Seager, M., Coulthard, A., Tennant, S., Buddles, M., Curtis, A. and Goodship, J.A. (2004) Identification of a mutation in synapsin I, a synaptic vesicle protein, in a family with epilepsy. *J. Med. Genet.*, **41**, 183–186.
34. Dravet, C. (2002) The behavioral disorders in epilepsy. *Rev. Neurol. (Paris)*, **158**, 4S33–38.
35. Tuchman, R., Moshe, S.L. and Rapin, I. (2009) Convulsing toward the pathophysiology of autism. *Brain Dev.*, **31**, 95–103.
36. Byers, P.H. (2002) Killing the messenger: new insights into nonsense-mediated mRNA decay. *J. Clin. Invest.*, **109**, 3–6.
37. Chin, L.S., Li, L., Ferreira, A., Kosik, K.S. and Greengard, P. (1995) Impairment of axonal development and of synaptogenesis in hippocampal neurons of synapsin I-deficient mice. *Proc. Natl. Acad. Sci. USA*, **92**, 9230–9234.
38. Sudhof, T.C. (2008) Neuroligins and neurexins link synaptic function to cognitive disease. *Nature*, **455**, 903–911.
39. Li, L., Chin, L.S., Shupliakov, O., Brodin, L., Sihra, T.S., Hvalby, O., Jensen, V., Zheng, D., McNamara, J.O. and Greengard, P. (1995) Impairment of synaptic vesicle clustering and of synaptic transmission, and increased seizure propensity, in synapsin I-deficient mice. *Proc. Natl. Acad. Sci. USA*, **92**, 9235–9239.
40. Takei, Y., Harada, A., Takeda, S., Kobayashi, K., Terada, S., Noda, T., Takahashi, T. and Hirokawa, N. (1995) Synapsin I deficiency results in the structural change in the presynaptic terminals in the murine nervous system. *J. Cell Biol.*, **131**, 1789–1800.
41. Terada, S., Tsujimoto, T., Takei, Y., Takahashi, T. and Hirokawa, N. (1999) Impairment of inhibitory synaptic transmission in mice lacking synapsin I. *J. Cell Biol.*, **145**, 1039–1048.
42. Valente, P., Casagrande, S., Nieus, T., Verstegen, A.M., Valtorta, F., Benfenati, F. and Baldelli, P. (2012) Site-specific synapsin I phosphorylation participates in the expression of post-tetanic potentiation and its enhancement by BDNF. *J. Neurosci.*, **32**, 5868–5879.
43. Medrihan, L., Cesca, F., Raimondi, A., Lignani, G., Baldelli, P. and Benfenati, F. (2013) Synapsin II desynchronizes neurotransmitter release at inhibitory synapses by interacting with presynaptic calcium channels. *Nat. Commun*. doi: 10.1038/ncomms2515.
44. Monaldi, I., Vassalli, M., Bachi, A., Giovedì, S., Millo, E., Valtorta, F., Raiteri, R., Benfenati, F. and Fassio, A. (2010) The highly conserved synapsin domain E mediates synapsin dimerization and phospholipid vesicle clustering. *Biochem. J.*, **426**, 55–64.
45. Hosaka, M., Hammer, R.E. and Sudhof, T.C. (1999) A phospho-switch controls the dynamic association of synapsins with synaptic vesicles. *Neuron*, **24**, 377–387.
46. Gitler, D., Cheng, Q., Greengard, P. and Augustine, G.J. (2008) Synapsin IIa controls the reserve pool of glutamatergic synaptic vesicles. *J. Neurosci.*, **28**, 10835–10843.
47. Pizzarelli, R. and Cherubini, E. (2011) Alterations of GABAergic signaling in autism spectrum disorders. *Neural Plast.*, **2011**, 297153.
48. Abbott, L.F. and Regehr, W.G. (2004) Synaptic computation. *Nature*, **431**, 796–803.
49. De Palma, M. and Naldini, L. (2002) Transduction of a gene expression cassette using advanced generation lentiviral vectors. *Methods Enzymol.*, **346**, 514–529.
50. Schneggenburger, R., Meyer, A.C. and Neher, E. (1999) Released fraction and total size of a pool of immediately available transmitter quanta at a calyx synapse. *Neuron*, **23**, 399–409.
51. Stevens, C.F. and Williams, J.H. (2007) Discharge of the readily releasable pool with action potentials at hippocampal synapses. *J. Neurophysiol.*, **98**, 3221–3229.
52. Bolte, S. and Cordelieres, F.P. (2006) A guided tour into subcellular colocalization analysis in light microscopy. *J. Microsc.*, **224**, 213–232.